Received: 15 August 2020 | Revised: 21 July 2021 | Accepted: 30 July 2021

DOI: 10.1111/gbb.12763

ORIGINAL ARTICLE

Genes, Brain and Behavior

Ccdc134 deficiency impairs cerebellar development and motor coordination

Sha Yin[1,2] | Qinyuan Liao[3] | Yida Wang[1,2] | Qianwen Shi[1,2] | Peng Xia[1,2] | Ming Yi[4] | Jing Huang[1,2]

[1]Department of Immunology, School of Basic Medical Sciences, Peking University, and NHC Key Laboratory of Medical Immunology (Peking University), Beijing, China

[2]Key Laboratory of Molecular Immunology, Chinese Academy of Medical Sciences, Beijing, China

[3]Department of Immunology, Guilin Medical University, Guilin, Guangxi province, China

[4]Neuroscience Research Institute and Key Laboratory for Neuroscience, Ministry of Education/National Health Commission of China, Peking University, Beijing, China

Correspondence
Ming Yi, Neuroscience Research Institute and Key Laboratory for Neuroscience, Ministry of Education/National Health Commission of China, Peking University, Beijing, China.
Email: mingyi@bjmu.edu.cn

Jing Huang, Department of Immunology, School of Basic Medical Sciences, Peking University, 38 Xueyuan Road, Haidian District, Beijing, China.
Email: huangjing82@bjmu.edu.cn

Funding information
National Natural Sciences Foundation of China, Grant/Award Number: 81974247; the Non-profit Central Research Institute Fund of Chinese Academy of Medical Sciences, Grant/Award Number: 2019PT320006

Abstract

Coiled-coil domain containing 134 (CCDC134) has been shown to serve as an immune cytokine to exert antitumor effects and to act as a novel regulator of hADA2a to affect PCAF acetyltransferase activity. While *Ccdc134* loss causes abnormal brain development in mice, the significance of CCDC134 in neuronal development *in vivo* is controversial. Here, we report that CCDC134 is highly expressed in Purkinje cells (PCs) at all developmental stages and regulates mammalian cerebellar development in a cell type-specific manner. Selective deletion of *Ccdc134* in mouse neural stem cells (NSCs) caused defects in cerebellar morphogenesis, including a decrease in the number of PCs and impairment of PC dendritic growth, as well as abnormal granule cell development. Moreover, loss of *Ccdc134* caused progressive motor dysfunction with deficits in motor coordination and motor learning. Finally, *Ccdc134* deficiency inhibited Wnt signaling but increased Ataxin1 levels. Our findings provide evidence that CCDC134 plays an important role in cerebellar development, possibly through regulating Wnt signaling and Ataxin1 expression levels, and in controlling cerebellar function for motor coordination and motor learning, ultimately making it a potential contributor to cerebellar pathogenesis.

KEYWORDS
Ataxin1, CCDC134, cerebellar development, granule cell, motor impairment, neural stem cell, proliferation, Purkinje cell, Wnt

1 | INTRODUCTION

Cerebellum morphogenesis is critically important for normal brain development. Cerebellar development is a systematic process that depends on neurogenesis, including migration and differentiation of neural stem cells (NSCs) and progenitor cells.[1] In particular, the appearance of granule cell progenitors (GCPs) on the surface of the cerebellum is a key feature of cerebellar development. GCPs undergo symmetric divisions after birth to generate the external granule layer (EGL), which peaks at postnatal day 7 and persists until the third week in mice, resulting in rapid cellular proliferation and differentiation.[2] Purkinje cells (PCs) located below the EGL control the proliferation of GCPs by releasing diffusible factors on approximately embryonic day 17.5 (E17.5) in mice.[3] The coordinated interaction between NSCs, GCPs, PCs and Bergmann glia cells (BGs) refines the developing cerebellum into the typical pattern of 10 folia and a three-layered cerebellar cortex, which includes the external molecular layer (ML), the middle Purkinje cell layer (PCL) and the innermost internal

Sha Yin, Qinyuan Liao and Yida Wang contributed equally to this work.

granular layer (IGL).[4] This developmental process and these well-defined cells in the cerebellum provide a highly suitable model to study neuronal properties and neural circuitry formation.

Developmental deficits of the cerebellum often result in motor and cognitive dysfunctions, including impaired coordination, balance, posture and skill learning, which have been linked to cerebellar ataxia and medulloblastoma, the most common pediatric brain tumor.[5,6] However, determining the molecular mechanisms of cerebellar development remains a great challenge of developmental neurobiology. Through the use of genetically modified mice, multiple genes have been implicated in the regulation of cerebellar development, such as fibroblast growth factor 8 (FGF8), reelin, gastrulation brain homeobox 2 (Gbx2), zinc finger protein 1/2 (Zic1/2), engrailed homeobox 1 (En1/2), receptor of activated protein kinase C1 (Rack1) and neurofibromin 1. In addition, the Wnt/β-catenin signaling is involved in GCP differentiation and cerebellar vermis formation.[7–9] However, the intracellular signaling pathways that coordinate and integrate those morphogenic signals are not well understood. Furthermore, the genetic pathways that determine the formation and patterning of cerebellar fissures remain unclear. Understanding the molecular mechanisms that underlie the complex development of the cerebellum will facilitate the development of novel treatment options for cerebellar disorders.

Coiled-coil domain containing 134 (CCDC134), a multifaceted scaffolding protein with a conserved coiled-coil domain, was originally identified as a classical secreted protein that inhibits Elk1 transcriptional regulation and the MAPK signaling pathway.[10] CCDC134 has been proposed as a cytokine-like molecule that exerts antitumor effects by augmenting $CD8^+$ T-cell mediated immunity,[11] and decreased expression of CCDC134 has been suggested as a candidate biomarker for malignant transformation in gastric cancer.[12] Meanwhile, CCDC134 is a novel regulator of human transcriptional adapter 2-alpha (hADA2α) and affects the acetyltransferase activity of the PCAF complex.[13] Mice lacking *Ccdc134* are embryonically lethal at the neurula stage, indicating the importance of this gene for mammalian brain development.[14] Nevertheless, the exact function of CCDC134 in the brain remains elusive. Intriguingly, *Ccdc134* loss leads to severe hemorrhages in the brain ventricular space and neural tube.[14] Thus, we hypothesize that CCDC134 might be critical for brain development.

In the present study, we show that CCDC134 is highly expressed in PCs during distinct stages of cerebellar development and plays a key role in cerebellar development. Ablation of CCDC134 expression in NSCs results in disruption of cerebellar morphogenesis, including a decrease in the number of PCs and impairment of its dendritic growth, consistent with the notion that CCDC134 inhibits granule cell development, ultimately leading to progressive motor dysfunction. Moreover, *Ccdc134* deficiency might inhibit Wnt signaling while increasing Ataxin1 levels.

2 | MATERIALS AND METHODS

2.1 | Mouse lines

The *Ccdc134*$^{fl/fl}$ and *Nestin-Cre* lines were used and genotyped as previously described.[14,15] Homozygous *Ccdc134*$^{fl/fl}$ mice were crossed with the Nestin-cre driver line. Conditional *Ccdc134* knockout (*Nestin-Cre*$^{+/-}$; *Ccdc134*$^{fl/fl}$, KO) mice were generated by second generation offspring, and *Nestin-Cre*$^{-/-}$; *Ccdc134*$^{fl/fl}$ (WT) mice were served as controls. All mice were on the C57BL/6J background. The mice were genotyped by PCR using murine tail DNA. All animal experiments were performed in accordance with protocols approved by the Institutional Animal Care and Use Committee for Peking University Health Science Center. All efforts were made to minimize suffering and to reduce the number of animals that were used.

2.2 | Human samples

Cerebellum tissue was provided by Guilin Judical Expertizing Center (GJEC). Informed consent for research purposes was obtained for brain autopsy and the usage of tissue and clinical information. The procedures of the GJEC are in accordance with all national laws and regulations and respect human rights. For this study, human cerebellum tissues were collected from 10 individuals in fetal (three cases, death because of inhalation of amniotic fluid at 38 or 39 weeks of gestation), child (three cases, aged from 5 months to 12 years, death from respiratory failure caused by pneumonia) and adult (four case, 21–44 years of age, death from carbon monoxide poisoning or sudden cardiac death) stages, and then processed according to standardized protocols.

2.3 | Histology and immunohistochemistry

For routine paraffin sectioning, whole brains were dissected after intracardiac perfusion with phosphate buffered saline (PBS) followed by 4% paraformaldehyde (PFA), and then fixed in 4% PFA at 4°C overnight, and then dehydrated through an ethanol series. The tissues were embedded in the proper orientation in paraffin and sectioned at a thickness of 20 μm using a microtome (Leica RM2245, Wetzlar, Germany). For frozen sections, tissues were fixed in 4% PFA at 4°C for 2 days and dehydrated in 20% sucrose at 4°C for 2 days followed by 30% sucrose solution for 2–5 days. The tissues were embedded with Tissue-Tek® OCT compound (Sakura, CA) and frozen in isopentane cooled by liquid nitrogen. Then, the tissue blocks were stored at −80°C and cytosectioned at a thickness of 20 μm using a microtome (Leica CM1900UV, Wetzlar, Germany). Routine hematoxylin and eosin staining, and Nissl staining were performed following described previously protocols.[16] The number of PC was counted, and data were presented as PCs per linear density in WT and *Ccdc134* KO group. The staining intensities were graded on the scale of 0, 1, 2 and 3, representing absent, weak, moderate and strong staining. These values were multiplied by the respective percentage of staining to obtain the H-scores ranging from 0 to 300.

For immunofluorescence staining, the cryosections were rehydrated and washed with PBS, blocked using 5% normal goat serum for 30 min at room temperature (RT). These slides were exposed to anti-CCDC134 (1:100, ab106442) and anti-NeuN (1:200, ab177487) purchased from Abcam Biotechnology (Cambridge, MA),

anti-calbindin (1:200, #13176), anti-neurofilament-L (1:200, #2837), anti-GFAP (1:200, #12389), anti-CNPase (1:200, #5664) from Cell Signaling Technology (CST, Boston, MA) and anti-Ataxin1 from Santa Cruz Biotechnology (1:50, sc-514,953, CA) at 4°C overnight. The slides were then washed with PBS and exposed to secondary antibody (1:200, Alexa 488-conjugated donkey-anti-mouse or Alexa 488-conjugated goat-anti-rabbit antibody, Thermo Fisher Scientific, Waltham, MA). For colocalization of CCDC134 and calbindin, the cryosections were incubated with anti-CCDC134 antibody at 4°C overnight, and then were stained with TRITC-conjugated goat-anti-rabbit antibody (1:400, ZSGB-BIO, Beijing, China) and Alexa Fluor 488-conjugated anti-calbindin (1:50, #65152S, CST, Boston, MA) for 2 h at RT. The sections were mounted using ProLong Diamond Antifade Reagent (P36961, Thermo Fisher Scientific, Waltham, MA). Sections were visualized and imaged with a fluorescence microscope (BZ-X700; Keyence, Osaka, Japan) or a confocal laser-scanning microscope (LSM 800; Carl Zeiss, Oberkochen, Germany). Cells were counted with ImageJ version 1.52.

2.4 | Western blot analysis

Cerebellar vermis and lung tissue as control were isolated and snap-frozen in liquid nitrogen and stored at −80°C. Tissues were homogenized with tissue isolation pestles using cell lysis buffer (10 mM Tris, pH 7.4, 1% Triton X-100, 150 mM NaCl, 1 mM EDTA) containing protease inhibitors cocktail (Roche, Basel, Switzerland). Protein concentrations were determined by Pierce™ BCA Protein Assay Kit (Thermo Fisher Scientific, Waltham, MA). A total of 50 μg of protein was subjected to a 12.5% SDS-polyacrylamide gel electrophoresis and blotted onto a nitrocellulose membrane. The membrane was blocked in 5% blocking grade milk for 1 h at room temperature. Primary antibodies were incubated overnight at 4°C for CCDC134 (1:1000), Ataxin1 (1:1000),[17] Calbindin (1:1000),[18] NeuN (1:1000), Axis inhibition protein 1 (Axin1, 1:1000, #2087),[19] phosphor-GSK-3α at Ser21 (1:1000, #8452),[20] phosphor-GSK-3β at Ser9 (1:1000, #5558),[21] β-catenin (1:1000, #8480),[22] which were purchased from Cell Signaling Technology (CST, Boston, MA) and β-actin (1:3000, M177-3, MBL, Nagoya, Aichi, Japan), followed by three washes in Tris-buffered saline with 1% Tween-20 and the appropriate secondary antibodies were incubated for 1 h at room temperature. Bands for Calbindin, NeuN, CCDC134, Axin1, Ataxin1, phosphor-GSK-3α at Ser21, phosphor-GSK-3β at Ser9 and β-catenin were visualized using Pierce™ ECL detection substrate (Thermo Fisher Scientific, Waltham, MA) and ImageQuant Las500 (Cytiva, Marlborough, MA), while the bands of β-actin as a loading control were analyzed using Odyssey Infrared Imaging System (LI-COR Biosciences, Lincoln, NE). The integrated volumes of appropriately sized bands were quantified using ImageJ software. Quantification of Calbindin, NeuN, CCDC134, Axin1, phosphor-GSK-3α (Ser21), phospho-GSK3β (Ser9), β-catenin and Ataxin1 levels was normalized to β-actin levels. Additionally, these antibodies used in immunoblotting experiments were validated in multiple research applications to ensure antibody performance, and the original pictures of the entire blot was shown in Figure S1. All analyses were performed twice in independent experiments.

2.5 | Behavioral testing

The rotarod and Morris water maze tests were performed on the same 8-week-old or 8-month-old male mice ($n = 6$), and three independent experiments were conducted. The rotarod test was performed to assess sensorimotor coordination and balance during the first and third weeks, and the Morris water maze test was used to evaluate spatial learning and memory abilities. Testing was conducted over 6 days, with at least a week between each test. Other behavior tests were performed on the same 8-week-old male mice ($n = 9$). Each test was conducted over 2 days, with at least 3 days between each test. All data were acquired and analyzed by an individual blinded to the genotypes.

2.6 | Rotarod test

Mice were trained on an accelerating rotating rod (5–40 rotations per minute over 2.5 min, MK-610A/RKZ; Muromachi Kikai, Tokyo, Japan) twice per day for 7 consecutive days, and the latency of the mice to fall after the training period was scored. The mice were allowed to rest between trials for at least 30 min. Average latency and speed during the testing phase were compared between WT and KO mice.

2.7 | Hind-paw clasping test

The test was performed as previously described.[23] The mice were grabbed near the base of their tails and suspended for a maximum time of 30 s. The position of the hind paws was scored as follows: "0," the hind paws were fully apart and away from the abdomen; "1," one hind paw were retracted near the abdomen for more than 10 s; "2," both hind paws were retracted near the abdomen for more than 10 s; "3," both hind paws were more than 80% retracted and almost touched the abdomen; "4," both hind paws were completely retracted, touching each other and the abdomen.

2.8 | Stationary beam test

The test apparatus consisted of a wooden beam (diameter = 2.5 cm, length = 50 cm) covered with a layer of masking tape to provide a firmer grip. A piece of cardboard was placed at each end to prevent the mice from escaping. Testing commenced by placing a mouse in the middle of the beam. The latency to fall was measured in two trials with an intertrial interval of 8 h. The latency was scored as 60 s if the mouse remained on the beam and then successfully climbed down the middle of the beam.

2.9 | Inversion test

For the inversion test of grip strength and endurance, mice were placed on a 4 cm × 4 cm iron screen (length and width = 20 cm) with mesh spacing that was sufficiently small to prevent the mice from escaping. The iron screen was turned upside down after the mouse grasped the iron screen firmly (10–30 s). The latency to the fall was measured in two trials with an intertrial interval of 8 h.

2.10 | Open field test

Locomotion was assessed by placing mice individually in the center of a Plexiglass chamber (40 cm × 40 cm × 30 cm), allowing them to explore for 30 min and observing the activity of mice in the center of the clear open-field apparatus. The total distance traveled, total vertical activity, the percentage of time active (defined as having a speed greater than 0.025 m/s) and the average speed while active were recorded using a HVS Image 2020 Plus tracking system (US HVS Image, San Diego, CA) connected to a camera mounted above the open-field chamber.

2.11 | Morris water maze

The Morris water maze apparatus consisted of a circular pool (height = 60 cm, diameter = 150 cm) filled with opaque water kept at 24°C. A round acrylic platform was placed in one quadrant. The mice were trained every day for 6 consecutive days; in each training trial, a mice mouse released from one of four different starting positions in a semirandom order, and the intertrial interval was 15 min. If a mouse was unable to reach the platform within 60 s, it was placed on the platform and kept there for 15 s before being returned to its home cage. The acquisition phase was followed by a probe trial during which the platform was removed from the maze, and the mice were allowed to swim freely for 120 s. The trajectories of the mice were recorded using a computerized video-tracking system. During the training trials, the escape latency to reach the platform and path lengths were recorded. During the probe trial, the quadrant exploration time and the number of times the mice crossed over the position of the original platform were evaluated.

2.12 | RNA sequencing analysis

Cerebella were excised from mice of each genotype and frozen in liquid nitrogen. Total RNA was isolated from cerebellar tissues with TRIzol reagent (Invitrogen, Waltham, MA) and subjected to RNA sequencing analysis using an Illumina sequencer in the sequencing and microarray facility of Shanghai NovelBio Bio-Pharm Technology Co., Ltd. The raw reads were aligned to the mm10 reference genome (build mm10) using Tophat2 RNA-seq alignment software. The mapping rate was 70% overall across all the samples in the data set. HTseq-Count was used to quantify the gene expression counts from the Tophat2 alignment files. Differential expression analysis was performed on the count data using the R package DESeq2. *p* values obtained from multiple binomial tests were adjusted using the false discovery rate. Significant genes were defined by a Benjamini–Hochberg-corrected *p* value cutoff of 0.05, and fold changes in RNA sequencing data were analyzed by Genesis and multiplot software.

2.13 | Quantitative real-time PCR

RNA was extracted from cerebella isolated from WT or KO mice with TRIzol reagent. cDNA was synthesized using a RevertAid First Strand cDNA Synthesis Kit (Fermentas, Thermo Fisher Scientific, Waltham, MA) following the manufacturer's instructions. The cDNA samples were subjected to quantitative PCR analyses using SYBR reagent (Roche, Basel, Switzerland). The expression of individual genes was calculated by the standard curve method and was normalized to the expression of Gapdh. The gene-specific primer sets used in this study (all for mouse genes) are listed in Table S1.

2.14 | Statistical analysis

All data are presented as the mean ± *SEM* and analyzed using Prism GraphPad software v8.0. Statistical analysis of two experimental groups was performed using two-tailed unpaired Student's *t* tests. Comparisons of three groups were performed using one-way analysis of analysis of variance (ANOVA) with Brown-Forsythe test followed by Tukey–Kramer post hoc tests, and comparisons of two groups with different time points were performed using two-way ANOVA with Geisser–Greenhouse correction followed by Dunn-Sidak post hoc tests. $p < 0.05$ as statistically significant.

3 | RESULTS

3.1 | Expression and localization of CCDC134 during mouse cerebellum development

We suspected that CCDC134 played a role in brain development, because our previous studies showed that *Ccdc134* deficiency led to subcutaneous hemorrhage and severe overall brain disorganization in the brain ventricular space in embryos.[14] Here, we first examined the expression of CCDC134 in human cerebellum autopsy specimens obtained from 10 individuals at fetal (three cases at 38 or 39 weeks of gestation), child (three cases, aged from 5 months to 12 years) and adult (four case, 21–44 years of age) stages. As shown in Figure 1A, relatively high CCDC134 expression levels were detected in PCs at all stages, and CCDC134 immunoreactivity in PCs at the fetal stage was highest but slightly decreased postnatally and remained constant thereafter (Figure 1C). Compared with the fetal stage, CCDC134 was expressed more broadly in the molecular layer and granular layer in child and adult stages, especially the deposition of extracellular CCDC134 in granular layer.

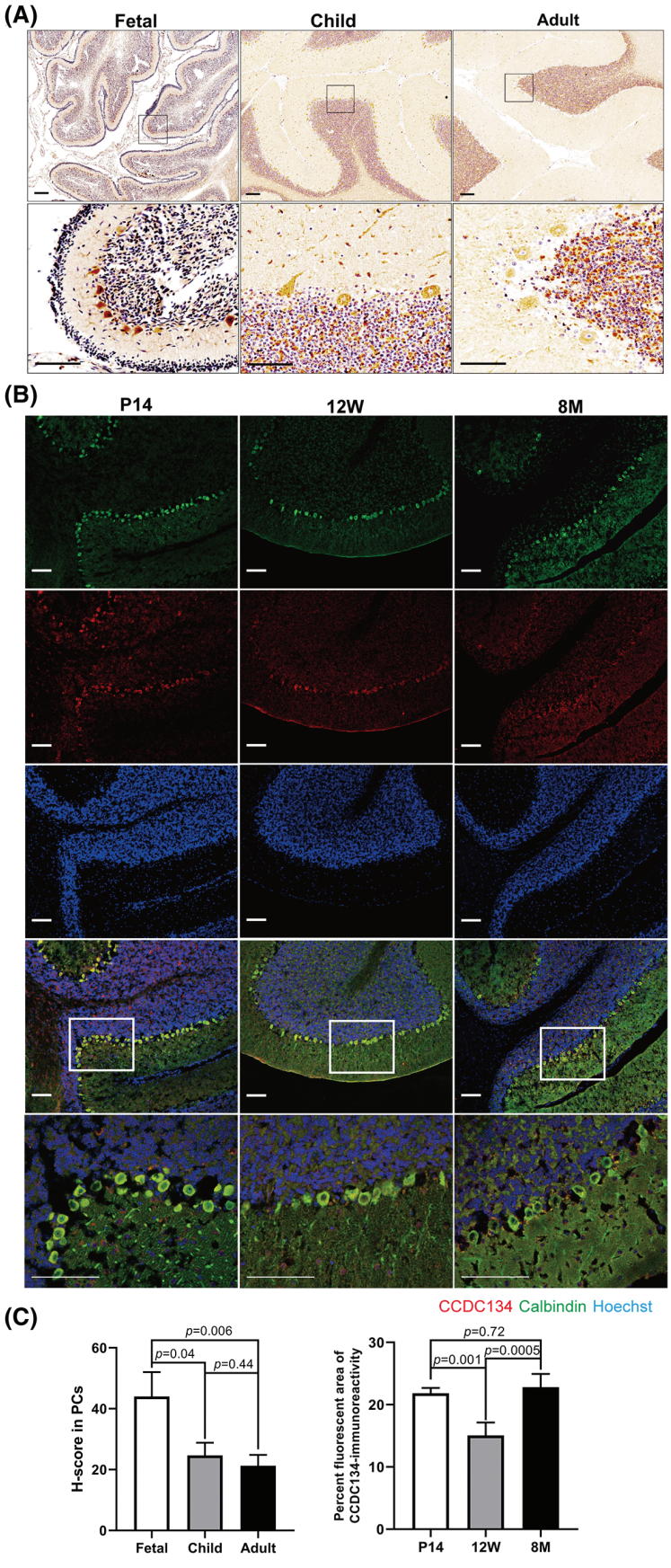

FIGURE 1 CCDC134 protein localization during cerebellar development. (A) Representative immunohistochemical staining of human cerebellar sections obtained from autopsy specimens of individuals at the fetal (38 weeks of gestation, $n = 3$), child (12 years of age, $n = 3$) and adult (42 years of age, $n = 4$) stages with specific antibody against CCDC134. High magnification showed specific localization of CCDC134 in PCs, molecular layer and granular layer of the cerebellum. Scale bar = 150 μm. (B) Representative immunofluorescence staining of cerebellum cryosections from P14, young and aged mice using CCDC134 (red), calbindin (green) and DAPI (blue). Scale bars = 100 μm. 12 W, 12-week-old mice; 8 M, 8-month-old mice. $n = 3$ per group. (C) Statistical analysis of CCDC134 immunoreactivity in cerebella was performed using one-way analysis of ANOVA with Tukey–Kramer post hoc tests. Data are shown as mean ± *SEM* from four different fields from three individuals per group. Distribution of the H-scores of CCDC134 in PCs of the human cerebellum at different stages (Left, $F_{2,7} = 10.84$, $p = 0.007$. fetal vs. child, $p = 0.04$; fetal vs. adult, $p = 0.006$; child vs. adult, $p = 0.44$). Semiquantitative image analysis of the percent fluorescent area of CCDC134-immunoreactivity in the cerebellum of mice at P14, young and aged adulthood stage (right, $F_{2,9} = 22.29$, $p = 0.0003$. p14 vs. 12 W, $p = 0.001$; p14 vs. 8 M, $p = 0.72$; 12 W vs. 8 M, $p = 0.0005$)

We also assessed the kinetics of the change in CCDC134 expression during mouse cerebellum development, which were consistent with the high cerebellar proliferation in early postnatal development. Sections of cerebella at different stages, including postnatal day 14 (P14) stage, young (12 weeks old) and aged (8 months old) stage, were immunostained with the specific antibody against CCDC134, and calbindin served as a marker of the PCs. CCDC134 signals were strong in the PC layer of the cerebellar cortex at all stages, where PC soma were localized. Compared with the postnatal stage, CCDC134 is also expressed more broadly in the molecular layer and granular layer in adult stages, especially the deposition of extracellular CCDC134 in aged stage (Figure 1B,C). Thus, CCDC134 may play a role during cerebella development.

3.2 | Ablation of *Ccdc134* in multipotent NSCs disrupts cerebellar development

Because constitutive *Ccdc134*-null mice are embryonic lethal,[14] the function of CCDC134 in neural development has remained elusive. To circumvent this caveat, we generated conditional *Ccdc134* knockout mice using the Cre-loxP system and bred *Ccdc134*$^{fl/fl}$ mice with *Nestin-Cre* transgenic mice, in which Cre recombination occurs in neuronal and glial precursors from E10.5 onward for targeting genes with brain region-restricted expression.[15] The structures of the different *Ccdc134* alleles are shown in Figure 2A. The CCDC134 disruption genotype was confirmed by PCR (Figure 2B). Next, the Nestin-cre-derived deletion of *Ccdc134* was further showed by CCDC134 mRNA level with RT-PCR (Figure 2C), and protein expression with western blotting (Figure 2D) and immunohistochemistry (Figure 2E). As expected, we observed a significant decrease in the expression of CCDC134 in cerebella tissue of cKO mice compared with those of WT mice, however, the visible bands were also detected in KO mice. In addition, we also used lung tissues of WT and KO mice as a control to verify the specific deletion of *Ccdc134* in mice cerebella tissue. Meanwhile, there existed nonspecific band at about 72 kDa and incomplete loss of CCDC134 protein in KO mice (Figure S1A), and it might be because of incomplete *Ccdc134* knockout with Nestin-cre driver targeting neural stem and progenitor cells.

The KO mice were viable and fertile, and the number of *Ccdc134* KO mice tended to be in accordance with the expected Mendelian ratio; however, the body weight of these mice was ~15% lower than

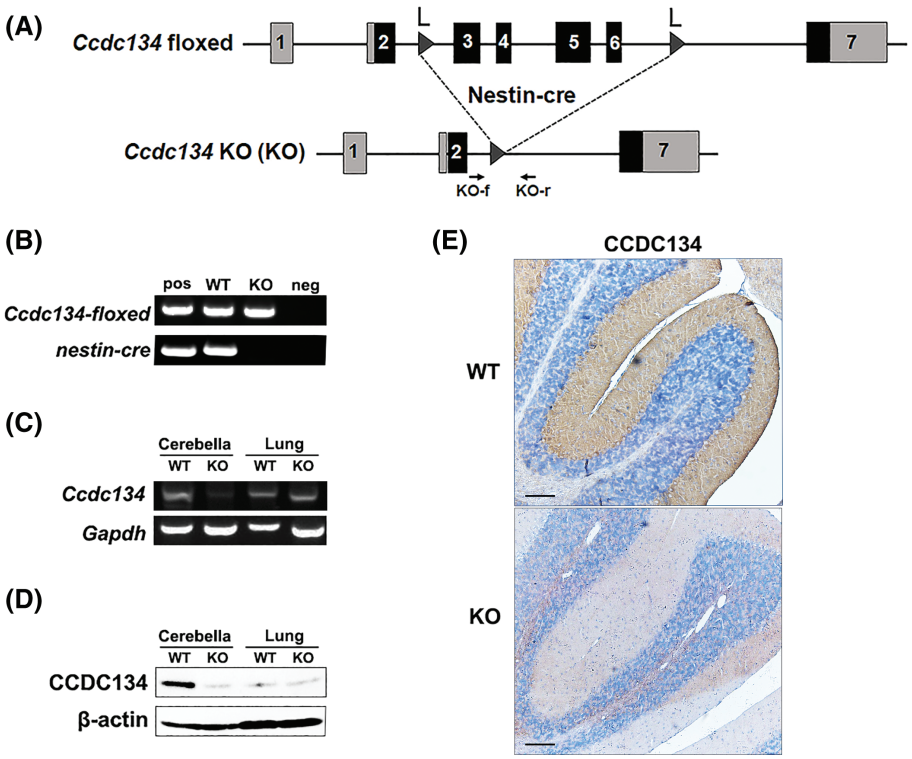

FIGURE 2 Generation of *Ccdc134* conditional knockout (*Nestin-Cre*$^{+/-}$: *Ccdc134*$^{fl/fl}$; KO) mice. (A) Schematic representation of the *Ccdc134* floxed allele following Cre recombination. The black arrows indicate the transcription start site, the black arrows indicate the location of the loxP primers (KO-f, KO-r), and the numbers indicate exons. (B) Typical PCR genotyping results are shown. The *Ccdc134* floxed allele (608 bp) was amplified by KO-f and KO-r. The Cre transgene (377 bp) was also detected by Cre-f and Cre-r. The sequences of the primers are provided in Table S1. pos, positive control. neg, negative control. (C) The *Ccdc134* mRNA level in WT and KO cerebellar tissue and lung tissue as control was detected. There was a gap of 380 bp between *Ccdc134* floxed alleles because of the elimination of exons 3 to 6 by Ccdc134-f and Ccdc134-r. (D) Western blot results comparing CCDC134 protein levels in WT and KO mice cerebellar tissue and lung tissue as control. CCDC134 was detected at ~26 kDa, and β-actin was used as an internal control. (E) Immunohistochemical staining of WT and KO cerebellar tissue was performed with a specific antibody against CCDC134. Scale bar = 100 μm. At least three samples were used from each group

that of WT mice during week 4, and the mice exhibited progressive weight loss until the age of 8 months (Figure 3A). It has previously been reported that the Nestin-Cre strain had a metabolic phenotype, which led to lower body weight phenotype, finally resulting in adult Nestin-Cre mice significantly lighter (11.2%) than littermate controls.[24] Given the potential side effects of Nestin-Cre strain, we further assessed the metabolic rate and respiratory quotient of *Ccdc134* KO and WT mice. Our results indicated that there was no obvious difference in these measured between *Ccdc134*-deficient mice and control mice (data not shown). Next, we also observed that *Ccdc134* KO mice also exhibited reductions in brain weight and size compared with WT littermates (Figure 3B). Since CCDC134 was expressed in the cerebellum, to determine whether cerebellar development was altered in KO mice, we compared the cerebella of 6-week-old *Ccdc134* KO mice with those of WT littermates. As shown in Figure 3B, the cerebella weight of *Ccdc134* KO mice significantly

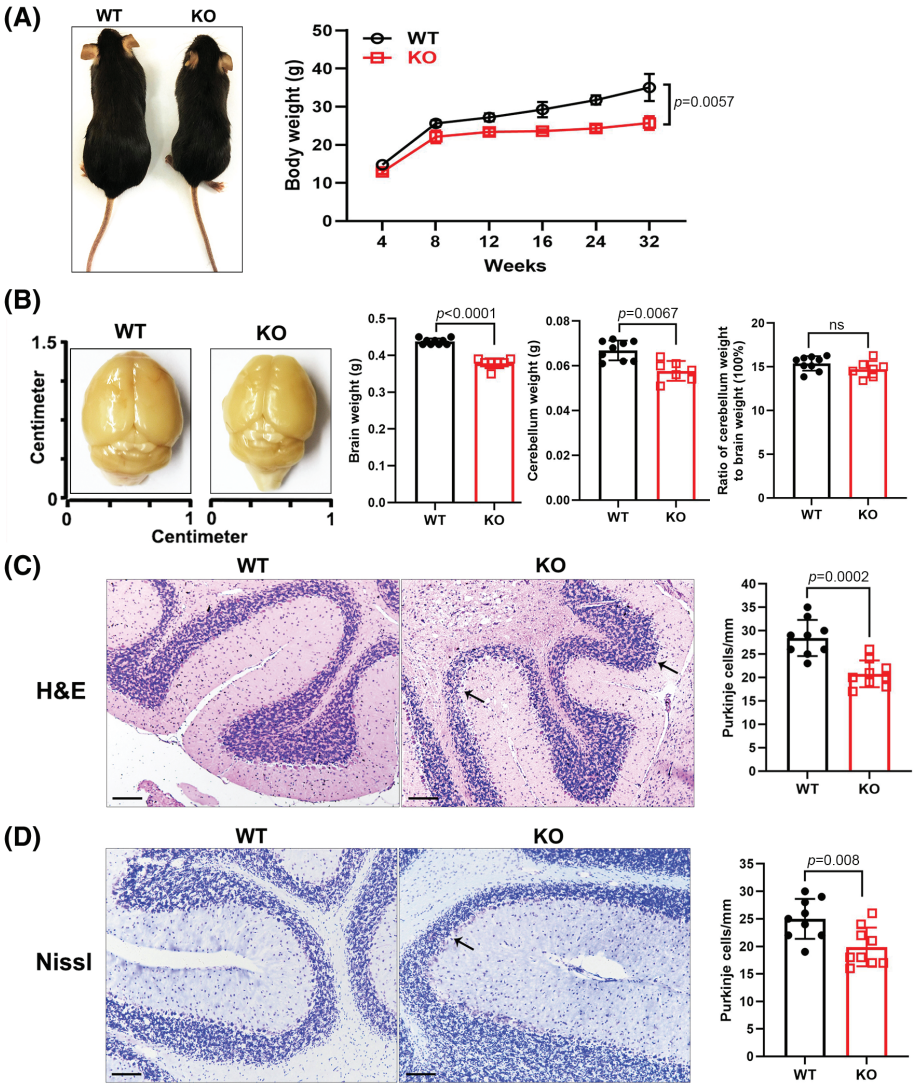

FIGURE 3 Conditional loss of *Ccdc134* in the brain results in morphological defects in the cerebellum. (A) Representative pictures of 6-week-old mice. Body size and body weight were reduced in *Ccdc134* KO mice compared with WT mice. Statistical analysis was performed by two-way ANOVA with Dunn-Sidak post-hoc tests ($p = 0.0057$; $n = 6$ per group for each time point. Group effect: $F_{1,10} = 121.7$, $p < 0.0001$; time effect: $F_{2,22} = 197.5$, $p < 0.0001$; interaction: $F_{5,48} = 11.28$, $p < 0.0001$). (B) Representative pictures of 6-week-old mouse brains. Brain size and brain weight were reduced in *Ccdc134* KO mice compared with WT mice. Statistical analysis of total brain weight, cerebellum weight and percent mass of cerebellum relative to the whole brain weight was performed by unpaired Student's *t* test ($n = 9$ for WT and $n = 7$ for KO group. Brain weight, $p < 0.0001$, $t = 10.85$, $df = 14$; Cerebellum weight, $p = 0.0067$, $t = 4.05$, $df = 6$; Ratio of cerebellum weight to brain weight, $p = 0.2682$, $t = 1.22$, $df = 6$). Representative images of HE staining (C) and Nissl staining (D) in the cerebellum of 6-week-old WT and *Ccdc134* conditional knockout (KO) mice. Sections were counterstained with eosin to visualize nuclei. Scale bar = 100 μm. Quantification of the number of Purkinje cells per linear density in KO and WT group was performed. Data are shown as mean ± *SEM* ($n = 9$ different fields from three mice per group). Statistical analysis was performed by unpaired two-tailed Student's *t* test (H&E staining, $p = 0.0002$, $t = 4.773$, $df = 16$; Nissl staining, $p = 0.008$, $t = 3.03$, $df = 16$). $p < 0.05$ considered significant. ns, not significant

reduced compared with WT group, however, the ratio of cerebella mass relative total brain weight showed no significant change. Moreover, the gross cerebellar morphology of KO mice was similar to that of the control mice, and KO mice exhibited developed vermis with well-defined lobes from birth to adulthood. Moreover, HE and Nissl staining of cerebellar midsagittal sections did not reveal gross abnormalities in foliation or organization of layers, but clear defects in PCs in the cerebellum were detected in adult KO mice compared with WT littermates (Figure 3C,D). These results suggest that *Ccdc134* depletion might lead to PCs defect during cerebellum development.

3.3 | Morphological defects in cerebellum of *Ccdc134*-deficient mice continue into adulthood

To test the notion that *Ccdc134* deletion results in morphological defects in the cerebellum, we next examined the organization of cerebellar granule cells and PCs in the cerebella of *Ccdc134* KO mice. We first examined PC organization and dendritic branching in the cerebella of WT and *Ccdc134* KO mice by immunostaining for calbindin, and we found that *Ccdc134* deletion led to PC loss and arborization defects (Figure 4A). Meanwhile, neurofilament-L was decreased in the cytoplasm of PCs and granular cells in the cerebella of *Ccdc134* KO

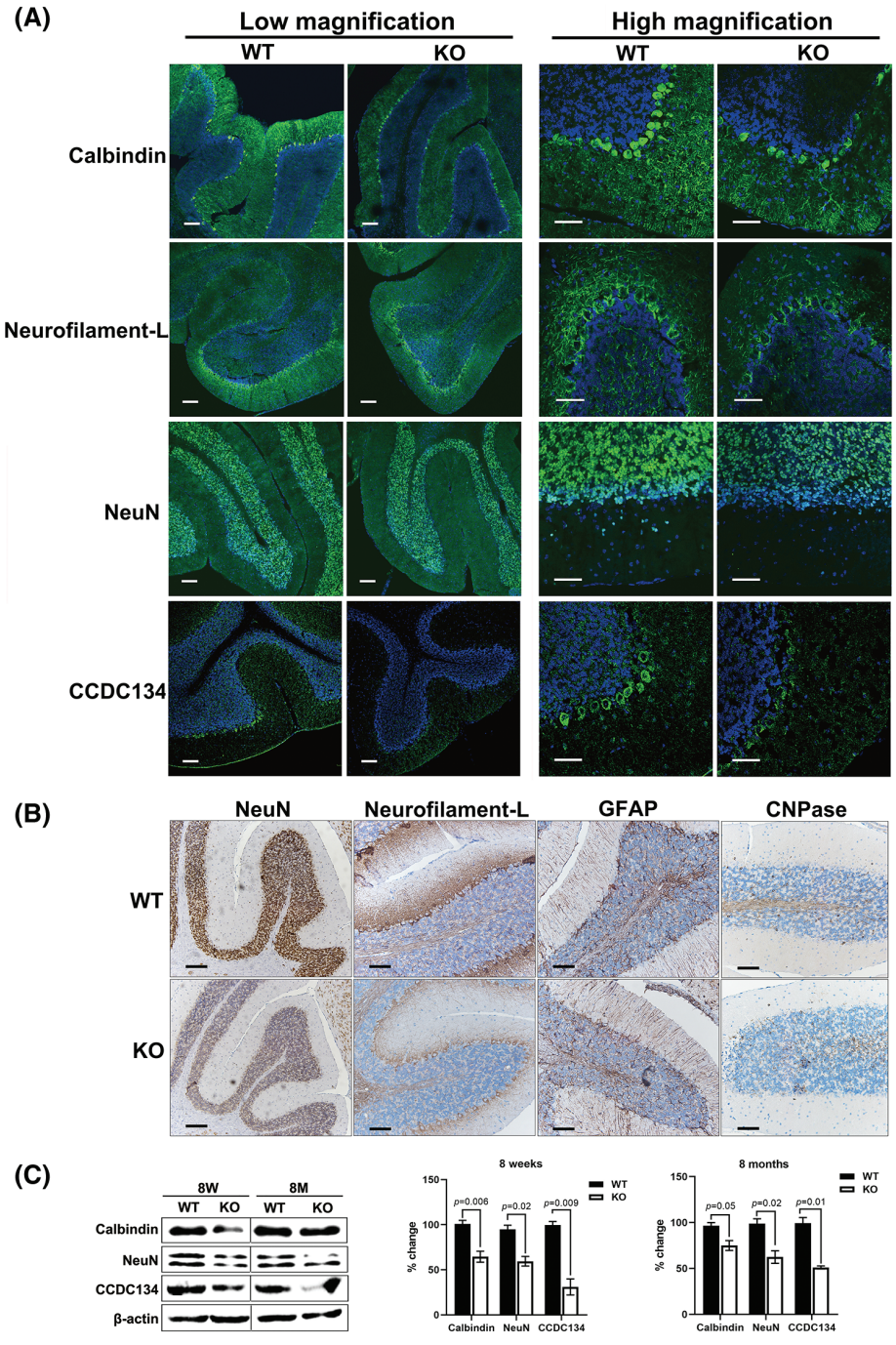

FIGURE 4 Morphological defects present in the cerebellum of *Ccdc134* deficient mice. (A) Representative immunofluorescence staining showing morphological and spatial distribution of calbindin (green) for PCs, neurofilament-L (green) for PCs and granular cells, NeuN (green) for postmitotic granule cells in the cerebella of 6-week-old *Ccdc134* KO and WT mice. DAPI (blue) was used for nuclear staining. Scale bars, 100 μm (low magnification) and 50 μm (high magnification). (B) Immunohistochemical staining for NeuN, neurofilament-L for neurons, GFAP for BGs and CNPase for oligodendrocytes in 8-week-old *Ccdc134* KO and WT mice. Scale bar = 100 μm. (C) Cerebellar fractions from both 8-week-old and 8-month-old *Ccdc134* KO and WT mice were probed with antibodies against calbindin, NeuN and CCDC134. β-actin was used as a loading control. The ratio of CCDC134, Calbindin or NeuN relative to β-actin each group was analyzed, and the histograms show the percentage change in protein expression in *Ccdc134* KO mice relative to WT controls. Statistical analysis was performed by unpaired two-tailed Student's *t* test. At least three samples were used from each group

mice compared with that of WT mice. Since granule cells continue to migrate into the IGL, PCs grow a dendrite that arborizes in the ML and occupies the space left by the migrating granule cells. We also observed the number of postmitotic granule cells with the panneuronal marker NeuN, which labels all postmitotic neurons with the exception of PCs,[25] and we found that there were significantly fewer NeuN-positive cells in the EGL and IGL of the *Ccdc134* KO mice cerebellum than the WT mouse cerebellum (Figure 4A). Deletion of *Ccdc134* in the brain was also confirmed by the lack of immunostaining in their cerebellum. These results were also confirmed by immunohistochemical staining of NeuN and neurofilament-L in *Ccdc134* KO mice cerebellum, where weaker staining was observed in KO mice compared with WT group (Figure 4B).

Since the endfeet of Bergmann glia form the glia limitans in the cerebellum, which together with the basal lamina build a barrier that insulates the cerebellum, and oligodendrocytes play a crucial role in nerve generation and myelination,[26] we compared the morphology of BGs and oligodendrocytes in the cerebella of WT and *Ccdc134* KO mice. However, no obvious differences in the density or general morphology of Bergmann glial cells, which are specifically labeled by glial acidic fibrillary protein (GFAP), or oligodendrocytes, which are specifically labeled by 2′,3′-cyclic nucleotide 3′-phosphohydrolase (CNPase), were detected (Figure 4B). Consistent with the immunofluorescent data, Western blot analysis revealed that cerebellar calbindin and NeuN protein expression levels were decreased in both 8-week-old and 8-month-old *Ccdc134* KO mice compared with WT mice (Figure 4C). It was interesting that there were two specific protein bands for NeuN, consisting of 46 and 48 kDa, which only existed in cerebellar tissue but not kidney tissue as control, suggest that there might exist protein modification for NeuN (Figure S1B). Meanwhile, there existed significant decrease but incomplete loss of CCDC134 protein in KO mice (Figure S1C). Together, these findings show that *Ccdc134* deficiency leads to impairment of PC and GC development and that the abnormal cerebellar phenotype apparent in *Ccdc134* KO mice persists into adulthood.

3.4 | *Ccdc134* deficiency impairs motor coordination and motor learning

Given that numerous studies have revealed a correlation between impairments in motor coordination and motor learning and disruptions in PC and granule cell elaboration,[27] we first tested the coordinated motor performance of the mice on an accelerating rotarod. Surprisingly, loss of *Ccdc134* impaired performance in the accelerating rotarod assay at both 8 weeks of age and 8 months of age. The WT mice quickly learned to balance themselves on the rod; however, the latency to fall of the *Ccdc134* KO mice was much shorter than that of the WT mice, although a slight improvement over time was observed (Figure 5A). Furthermore, there were significant differences in the latency to first fall of the WT and *Ccdc134* KO mice in the inversion test and stationary beam test, which assessed grip strength and endurance (Figure 5B). Moreover, *Ccdc134* KO mice exhibited hind paw clasping when suspended by the tail (Figure 5D), a sign of neurological dysfunction.[23]

Furthermore, we evaluated spatial learning and memory abilities in 8-week-old and 8-month-old WT and *Ccdc134* KO mice using the Morris water maze task. The latency to reach the platform was increased in 8-week-old *Ccdc134* KO mice compared with 8-week-old WT mice. However, no significant differences in frequency of platform crossings or mean velocity were observed between 8-week-old WT mice and 8-week-old *Ccdc134* KO mice (Figure S2A). Furthermore, we observed that 8-month-old *Ccdc134* KO mice displayed a significantly longer latency to reach the platform, a lower frequency of platform-crossings and a slower mean velocity than WT controls (Figure 5Eshowing that *Ccdc134* deficiency might lead to abnormal spatial learning and memory. We next asked whether CCDC134 can influence anxiety-like or depression-like behavior. As shown in Figure 5F, open field test indicated that *Ccdc134* KO mice displayed slightly less vertical activity in the open-field chamber, spent more time in its center and traveled a shorter distance over 5 min than WT mice. However, no significant differences were found between *Ccdc134* KO and WT mice using elevated plus maze (EPM), sucrose preference test (SPT), forced swim test (FST) and tail suspension test (TST) (Figure S2B–E). The results suggest that *Ccdc134* deficiency mainly causes progressive loss of motor coordination, probably also led to abnormal anxiety-related behavior.

3.5 | *Ccdc134* deletion decreased cell differentiation and proliferation via the Wnt signaling pathway

To explore the genes involved in *Ccdc134* deficiency and the resultant abnormal cerebellar phenotype, RNA-seq analysis was carried out in the cerebella of WT and *Ccdc134* KO mice. Differential expression analysis started with low-expression filtering, which resulted in the identification of 13,156 genes (having a CPM >1 in three samples). These differentially expressed genes included 97 in the cerebellum. A heat map was used to show the intensities of the expression of each gene (Figure 6A). To obtain a sufficient number of differentially expressed genes, a relaxed cut-off was used (significance at $p < 0.05$ and an absolute fold change >2) for all statistical functional enrichment analyses. Significant KEGG categories included cerebellum development, cell differentiation and proliferation and the Wnt signaling pathway. As might be expected, CCAAT/enhancer-binding protein δ (Cebpd), a transcription factor that is a member of the CCAAT/enhancer-binding protein family, is expressed in the brain throughout development and into adulthood and has been shown to play regulatory roles in neuroinflammation, learning, and memory, was downregulated in the cerebellum.[28,29] Other transcription factors, such as storkhead box 1 (Stox1), which is a forkhead transcriptional factor that plays a pivotal role in cerebellar granule neurogenesis is upregulated along with GCP differentiation and repressed by activation of sonic hedgehog (SHH) signaling, were differentially expressed.[30]

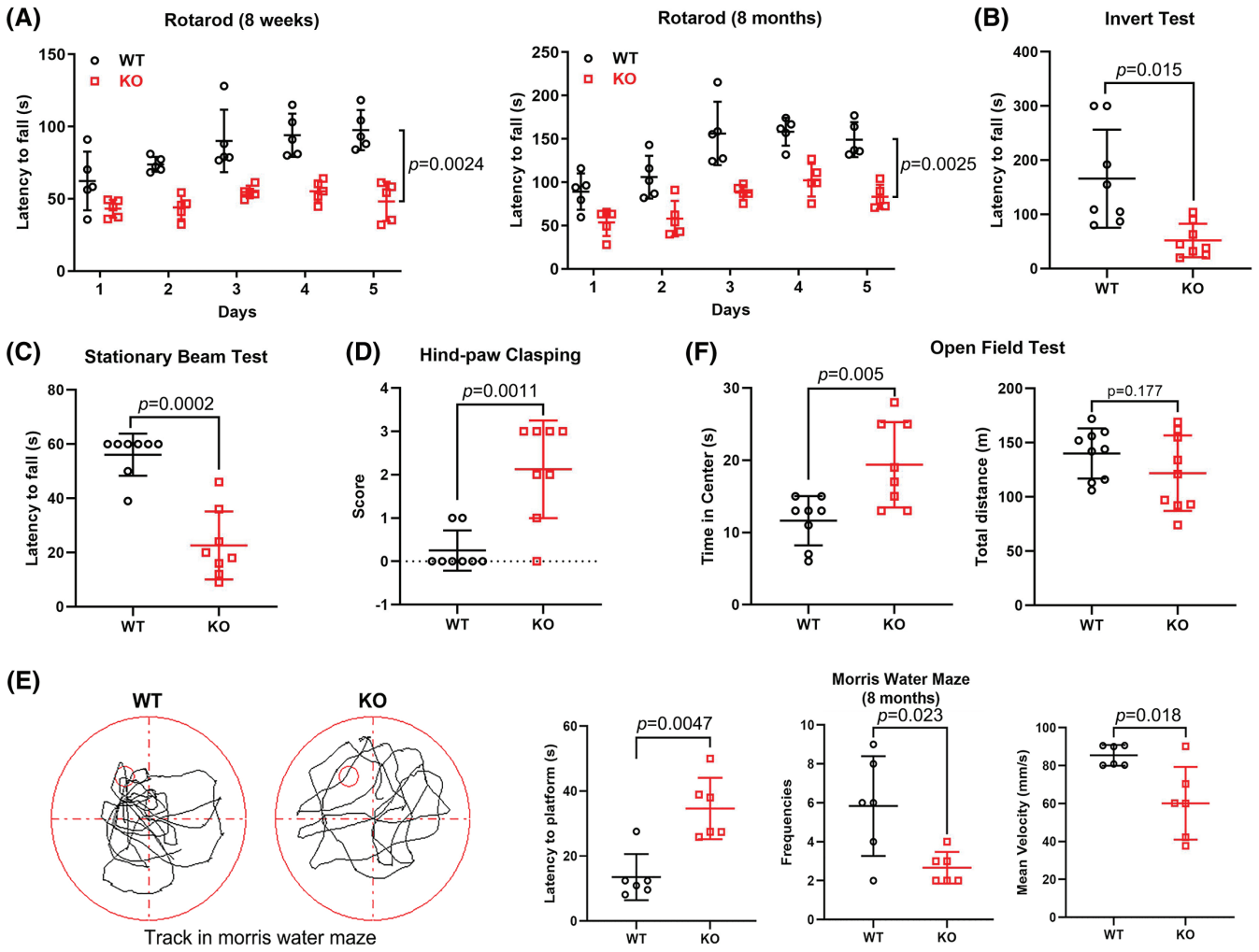

FIGURE 5 *Ccdc134* knockout mice develop progressive motor and cognitive function deficits. The representative result was shown, and behavioral tests were repeated at least three times using 8-week-old male mice per group. (A) Accelerating rotarod test. Mice were trained over 5 days. The performance of the *Ccdc134* KO mice was significantly different from that of WT mice from day 1; by day 2, the difference between the WT and *Ccdc134* KO mice was statistically significant, as analyzed by two-way ANOVA with Dunn-Sidak post hoc tests ($n = 6$ per group. For 8-week-old mice: $p = 0.0024$, group effect: $F_{1,8} = 98.66$, $p < 0.0001$; time effect: $F_{2,14} = 5.59$, $p = 0.018$; interaction: $F_{4,32} = 1.78$, $p = 0.16$. For 8-month-old mice: $p = 0.0025$, group effect: $F_{1,8} = 63.13$, $p < 0.0001$; time effect: $F_{3,23} = 13.89$, $p < 0.0001$; interaction: $F_{4,32} = 1.15$, $p = 0.35$). (B) Analysis of the performance of WT and *Ccdc134* KO mice in the inversion test by unpaired two-tailed Student's *t* test ($n = 9$ per group, $p = 0.015$, t = 3.221, $df = 7$). (C) Analysis of the performance of WT and *Ccdc134* KO mice in the stationary beam test by unpaired two-tailed Student's *t* test ($n = 9$ per group, $p = 0.0002$, t = 6.942, $df = 7$). (D) Analysis of hind paw clasping of the mice. A higher score indicates a more severe phenotype. Statistical analysis was performed by unpaired two-tailed Student's *t* test ($n = 9$ per group, $p = 0.0011$, t = 5.351, $df = 7$). (E) The Morris water maze test was performed on 8-month-old WT and *Ccdc134* KO mice. Training was conducted over 5 days, with two training trials per day, and the latency to reach the platform was analyzed. The platform is marked by a white pointed circle in the first quadrant. Representative schematic of mouse trajectories in the Morris water maze test are shown (left). Statistical analysis was performed by unpaired two-tailed Student's *t* test ($n = 6$ per group, latency to the platform, $p = 0.0047$, t = 4.85, $df = 5$; frequency of platform location crossings, $p = 0.023$, t = 3.23, $df = 5$; mean swimming velocity, $p = 0.018$, t = 3.442, $df = 5$). (F) Total traveled distance and time spent in the center of the open-field arena over a 1-min period are displayed for 8-week-old WT and *Ccdc134* KO mice. Statistical analysis was performed by unpaired two-tailed Student's t-test (n = 9 per group, *Time in center*, $p = 0.005$, t = 5.351, $df = 7$; Total distance, $p = 0.177$, t = 5.351, $df = 7$). $p < 0.05$ considered significant. ns, not significant

To validate the expression changes identified by RNA-seq analyses, selected genes were examined in more detail by quantitative real-time PCR (qRT-PCR). The alterations in the gene expression of *Hspa5*, *Tdo2*, *Cebpd*, *Stox1*, *Canx* and *Wif1* directly corresponded with the specific RNA-seq data, for example, decreases in *Tdo2*, *Cebpd*, *Stox1* and *Canx* mRNA and increases in *Hspa5* and *Wif1* mRNA were found in the cerebella of *Ccdc134* KO mice compared with the cerebella of WT controls (Figure 6B). Immunohistochemical staining for glutamate decarboxylase 67 (GAD67), a GABA synthesizing enzyme highly correlated with changes in the PCs, showed weaker GAD67 expression in the somata and dendrites of PCs and the ML of the cerebella in *Ccdc134* KO mice than in WT mice (Figure 6C). These results

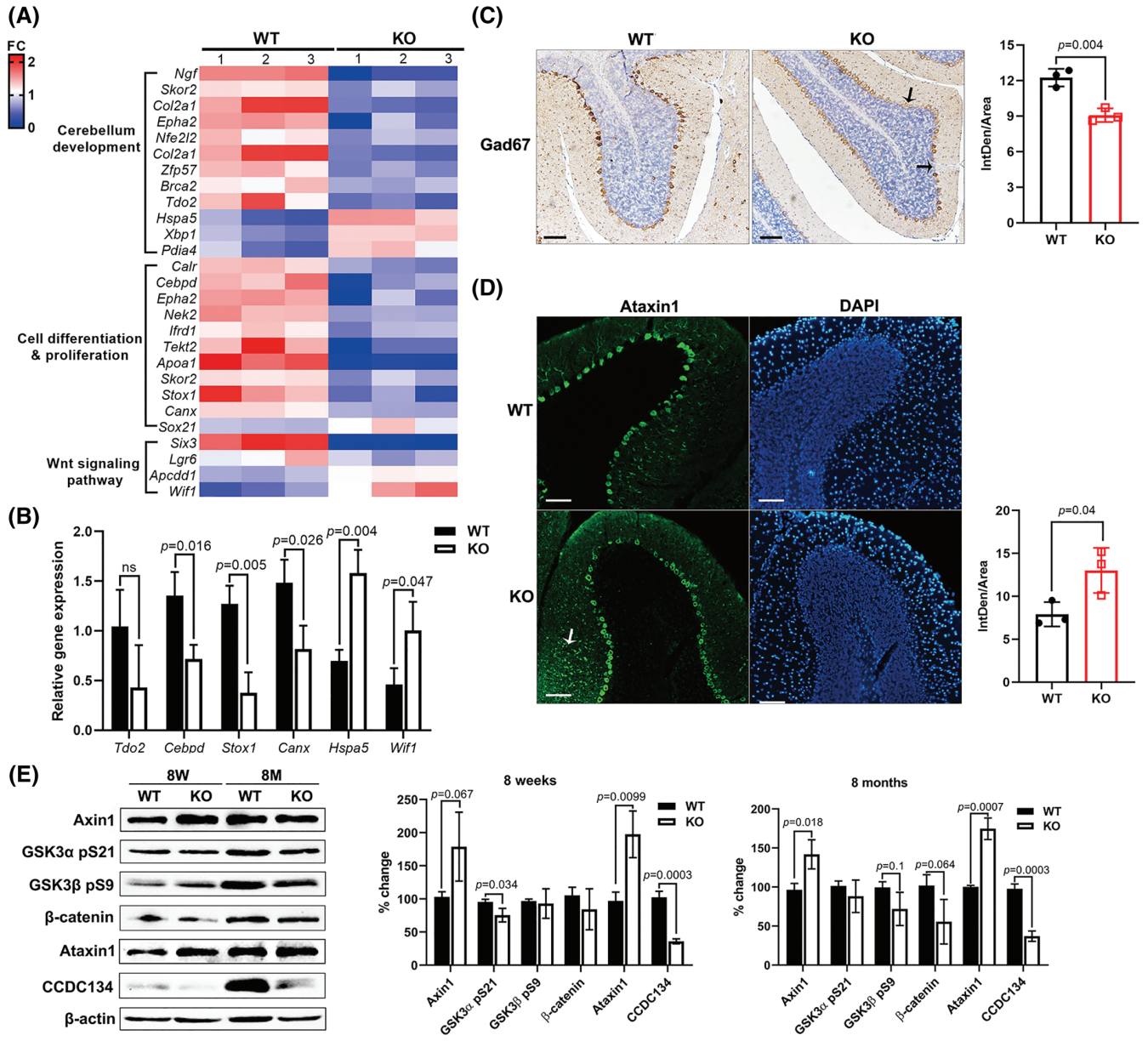

FIGURE 6 *Ccdc134* deletion inhibits cell proliferation and the Wnt signaling pathway. (A) Cerebellar tissues were isolated from 8-week-old WT and *Ccdc134* KO mice ($n = 3$ per group) and subjected to RNA-seq analysis. The heat maps show fold changes (FC) in expression using a cut-off of $p < 0.05$ and requiring an absolute fold change of above 2. (B) RNA was extracted from the cerebellar tissues of 8-week-old WT and *Ccdc134* KO mice. qRT-PCR was performed, and the expression levels were normalized to the level of Gapdh. *Ccdc134* KO mice expressed lower levels of *Tdo2*, *Cebpd*, *Stox1* and *Canx* but higher levels of *Hspa5* and *wif1* than WT mice. Values from three independent experiments with at least three biological replicates were used, and statistical analysis was performed by unpaired two-tailed Student's *t* test ($n = 3$ per group, *Tdo2*, $p = 0.13$, t = 1.9, $df = 4$; *Cebpd*, $p = 0.016$, t = 3.99, $df = 4$; *Stox1*, $p = 0.005$, t = 5.62, $df = 4$; *Canx*, $p = 0.026$, t = 3.47, $df = 4$; *Hspa5*, $p = 0.004$, t = 5.84, $df = 4$; *Wif1*, $p = 0.047$, t = 2.83, $df = 4$). (C) Representative immunohistochemistry images of cerebellar Purkinje cells of 8-week-old *Ccdc134* KO and WT mice stained with an antibody against Gad67. Scale bar = 100 μm. (D) Representative images of immunofluorescence confocal microscopy of Ataxin1 (green) and DAPI (blue) in the cerebella of 8-week-old *Ccdc134* KO and WT mice. Increased Ataxin1 expression was observed in the KO mice compared with WT group. Scale bar = 50 μm. Quantification of fluorescence intensity for the Gad67 and Ataxin1 immunohistochemistry in the cerebellum was performed. Data are shown as mean ± *SEM* (Average of four different fields per mice) from three mice per group. Statistical analysis was performed by unpaired two-tailed Student's *t* test (*Gad67*, $p = 0.004$, t = 5.86, $df = 4$; Ataxin1, $p = 0.04$, t = 2.97, $df = 4$). (E) Cerebellar fractions from both 8-week-old and 8-month-old *Ccdc134* KO and WT mice were probed with antibodies against Axin1, phosphor-GSK3α (Ser21), phospho-GSK3β (Ser9), β-catenin, Ataxin1 and CCDC134. β-actin was used as a loading control. Quantification of Axin1, GSK3α pS21, GSK3β pS9, β-catenin, Ataxin1 and CCDC134 levels normalized to β-actin levels. At least three samples were used from each group. Statistical analysis was performed between *Ccdc134* KO and WT mice by unpaired Student's *t* test. $p < 0.05$ considered significant. ns, not significant

were consistent with the results of RNA-seq analysis and showed that cerebellar granule cells and PCs are impaired in response to *Ccdc134* deficiency during cerebellar development. Other study gives a clue that CCDC134 was identified to interact with A1Up (Ataxin-1 interacting ubiquitin-like protein), which interacts with and co-localizes with Ataxin-1 in PCs using a stringent protein–protein interaction network to reveal common cellular pathways that might lead to PC dysfunction and degeneration.[31] Our result also indicated that the expression of Ataxin1, another polyglutamine-containing protein that is predominantly expressed in the nucleus but is sometimes expressed in the cytoplasm of PCs,[32] was elevated and aggregated in the ML of in the cerebella of *Ccdc134* KO mice compared with the cerebella of WT control mice (Figure 6D). In addition, the increasing expression of Ataxin 1 was detected in the cerebella of both 6-week-old and 8-month-old *Ccdc134* KO mice compared with control mice using western blotting (Figure 6E).

Having determined a central role of CCDC134 in cerebellar development, we next explored the underlying CCDC134-mediated Wnt/β-catenin signaling pathway in cerebella of 6-week-old and 8-month-old WT and KO mice, and the result showed that *Ccdc134* depletion negatively regulated Wnt/β-catenin signaling pathway, including the elevated level of Axin1 expression but decreased levels of active form of GSK-3α and GSK3β, as well as reduced β-catenin expression in *Ccdc134* KO mice compared with the cerebella of control mice (Figure 6E). These results suggest that CCDC134 plays a role in cerebellar development, possibly through regulating Wnt signaling and Ataxin1 expression levels, and in controlling cerebellar function for motor coordination and motor learning.

4 | DISCUSSION

This study reveals the role of CCDC134 in central nervous system using a mouse line in which *Ccdc134* deletion was restricted to NSCs. We observed a reduced brain size, a decreased number of PCs and stunted PC dendrites in conditional *Ccdc134* KO mice compared with WT mice. These phenotypes of the mutant cerebellum indicate that CCDC134 might be critical for cerebellar development.

Our previous study showed that hemorrhages occur in the brain ventricular space and neural tube, resulting in severe overall brain disorganization and embryonic lethality from embryonic day 12.5 to birth in homozygous *Ccdc134* knockout mouse embryos, but not in littermates.[14] In the present study, immunostaining using a specific anti-CCDC134 antibody was performed on sections of human cerebellar autopsy specimens and frozen cerebellar sections from wild-type mice at embryonic, adolescent and adult stages. We found that the CCDC134 protein was highly expressed in the PCs soma. Moreover, there was a decreased number of PCs and stunted PC dendrites in *Ccdc134* knockout mice compared with wild-type mice. All of the above data provide evidence that CCDC134 might play an important role during cerebellar development.

The cerebellar cortex contains distinct cell types that are positioned in a typical layered pattern. Among these cells, PCs act as the sole output neurons of the cerebellar cortex during cerebellar development and secrete sonic hedgehog (Shh) to induce GCP proliferation.[33] Since perpetual proliferation of GCP during the first postnatal days leads to the formation of the EGL, a large number of granule cells migrate from the EGL to the IGL along Bergmann glial cell processes between P5 and P10, and PCs grow a dendrite that arborizes in the molecular layer and occupies the space left by the migrating granule cells.[26] In addition, all Bergmann glial cells are arranged around the cell bodies of Purkinje neurons, PCs also use Bergmann glial processes as a guide as they grow into the base of the EGL,[34] at which point Bergmann glial cells form a scaffold for migrating granule cells.[35] We observe that mice lacking CCDC134 displayed significant decreases in PCs specific for calbindin and postmitotic granule cells specific for NeuN, while no obvious differences in Bergmann glial cells were observed. Thus, CCDC134 might mainly inhibit granule cell migration by regulating PC development, which in turn, determines the cerebellum development.

Since PCs are essential for the motor coordination of the body, motor dysfunction is frequently caused by the altered function of PCs. *Ccdc134* knockout mice display progressive motor incoordination, hind-paw clasping and reduced exploratory activity and kinematic learning ability, which correlate with cerebellar histology and physiology. When mice were subjected to motor coordination tasks involving a rotating rod, the latencies of *Ccdc134* KO mice, unlike those of controls, did not appear to improve over five trials, which could indicate deficits in motor learning in addition to motor coordination. Many studies have indicated that such motor deficits often involve disruptions in PC elaboration.[36] Similarly, the decreases in mean velocity and frequencies observed in the Morris water maze are consistent with those observed in other rodent models with cerebellar defects, and these behavioral abnormalities are likely attributed to cerebellar impairment.[37,38] It is not surprising that the loss of PCs in the cerebellum can impact granule-PC connectivity and ultimately result in motor defects. The persistence of motor deficits into adulthood after cerebellar development and growth is complete. Further work should examine whether connectivity or signaling between granule and PCs is aberrant using cell-specific mouse models. Besides these, we also observed *Ccdc134* deficiency led to abnormal anxiety-related behavior, which is related to non-cerebellar regions. Thus, these abnormal behaviors of *Ccdc134* knockout mice are most likely induced by the functional and structural defects of the cerebellum but probably related to other non-cerebellar regions.

Our data clearly indicated that the body weight of KO mice was approximately 15% lower than that of WT mice during week 4, and then exhibited progressive weight loss until the age of 8 months. Since Nestin-Cre transgenic mice were found to have smaller body weights than littermate controls, which is probably related to the fact that this Cre line is affected by mild hypopituitarism.[24] Thus, the phenotype of weight loss might be because of the potential side effects of Nestin-Cre strain, masking the effect of the *Ccdc134* deletion itself. It has been reported that Nestin-Cre mice have overall response to stimuli triggering anxiety-like behaviors but a strong impairment in the

acquisition of both contextual- and cued-conditioned fear, but no alterations in locomotion, general exploratory activity, learning and memory, sociability, startle response and sensorimotor gating was observed in Nestin-Cre mice.[39] However, *Ccdc134* KO mice displayed impaired motor coordination and motor learning, as well as abnormal anxiety-related behavior, compared with WT mice, suggesting that *Ccdc134* deletion itself contributes to abnormal cerebellar development. In addition, we also found incomplete knockout of *Ccdc134* after crossing with Nestin-Cre mice. Other studies also showed that there were incomplete knockout of targeted molecules using Nestin-cre driver, such as TCTP and Fpn1,[40,41] suggesting that Nestin-cre driver targeting neural stem and progenitor cells, might lead to a significant decrease in the expression of targeted molecules in neuronal cells of cKO mice but not reach complete gene knockout.

Several lines of evidence have revealed that the correct type, location and number of neurons results from the interplay of various signaling molecules and transcription factors to ensure proper cerebellar development. One of the key signaling pathways that are known to exert crucial roles in regulating various aspects of neurogenesis is Wnt signaling.[42] Wnt signaling proteins are lipid modified glycoproteins that are highly conserved among various species. In the cerebellum, Wnt/β-catenin signaling has been shown to promote the proliferation of ventricular zone progenitors and impair their differentiation during early development.[43,44] Additional support for the role of Wnt/β-catenin signaling in cerebellar development comes from its association with cerebellar-associated tumors and medulloblastoma. Significant KEGG categories from RNA-seq analysis included cerebellum development and cell differentiation and proliferation as well as the Wnt signaling pathway. Among the genes related to Wnt signaling, the homeobox gene *Six3*, which is expressed during forebrain and visual system development, is dynamically downregulated in *Ccdc134* KO mice.[45] Germ line inactivation of Six3 in mice causes truncation of the forebrain and rostral expansion of Wnt1.[46] Haploinsufficiency of Six3 fails to activate Shh expression in the ventral forebrain and causes holoprosencephaly.[47] Similarly, adenomatous polyposis coli down-regulated 1 (Apcdd1), a membrane-bound glycoprotein with a highly conserved cysteine-rich region in its extracellular domain, is both a downstream target and inhibitor of the canonical Wnt pathway. Apcdd1 blocks the interaction between Wnt3A and low-density lipoprotein receptor-related protein 5 (Lrp5), thus inhibiting downstream stabilization of β-catenin and several Wnt-mediated developmental processes including embryonic axis specification and neural proliferation.[48] In addition, both Wif1 and Lrg6 contribute to Wnt signaling.[49] We also detected that *Ccdc134* depletion negatively regulated Wnt/β-catenin signaling pathway. All of the above data suggest that CCDC134 might regulate Wnt signaling, which coordinates cerebellar development.

The deficits we observed in the *Ccdc134* KO mice, such as progressive motor incoordination, hind-paw clasping and PC and dendritic degeneration, are typical features of spinocerebellar ataxin type 1 (SCA1), a disease that causes progressive loss of motor control in patients.[32] Our results reveal that *Ccdc134* KO mice display elevated levels of Ataxin1 and develop even more severe PC pathology, showing significant loss of PCs dendritic after 8 months. Ataxin1 is a polyglutamine-containing protein that causes SCA1 and is expressed throughout the brain from very early embryonic stages.[50] Notably, CCDC134 is a scaffolding protein localized within the cytoplasm and nucleus,[13] and how this intracellular protein can affect PC development by regulating ataxin1 modification requires further investigation. In conclusion, we propose that identifying molecules capable of regulating Ataxin1 levels may provide insight into factors that contribute to cerebellar degeneration.

That is the first study to show an essential role for CCDC134 in cerebellar development. *Ccdc134* deletion decreases the size of the cerebellum and induces symptoms of cerebellar ataxia, either as a direct effect of PC loss or indirectly through inhibiting GCP proliferation. CCDC134 is required for PC development, possibly through regulation of the Wnt signaling pathway. *Ccdc134* deletion reduces the levels of Gad67 and increases the levels of Ataxin1. Thus, the function and molecular mechanism of CCDC134 will be explored to further elucidate normal cerebellar neurogenesis and circuit formation and identify processes that are likely dysregulated in many cerebellum-associated developmental disorders and pediatric cerebellar tumors such as medulloblastoma.

ACKNOWLEDGMENT

This work was supported by the National Natural Sciences Foundation of China (81974247) and the Non-profit Central Research Institute Fund of Chinese Academy of Medical Sciences (2019PT320006).

CONFLICT OF INTEREST

The authors declare that they have no competing interests.

DATA AVAILABILITY STATEMENT

The data that support the findings of this study are available from the corresponding author upon reasonable request.

ORCID

Jing Huang https://orcid.org/0000-0002-0814-838X

REFERENCES

1. Goldowitz D, Hamre K. The cells and molecules that make a cerebellum. *Trends Neurosci*. 1998;21:375-382.
2. Espinosa JS, Luo L. Timing neurogenesis and differentiation: insights from quantitative clonal analyses of cerebellar granule cells. *J Neurosci*. 2008;28:2301-2312.
3. Smeyne RJ, Chu T, Lewin A, et al. Local control of granule cell generation by cerebellar Purkinje cells. *Mol Cell Neurosci*. 1995;6:230-251.
4. Butts T, Green MJ, Wingate RJ. Development of the cerebellum: simple steps to make a 'little brain'. *Development*. 2014;141:4031-4041.
5. Beckinghausen J, Sillitoe RV. Insights into cerebellar development and connectivity. *Neurosci Lett*. 2019;688:2-13.
6. Hatten ME, Roussel MF. Development and cancer of the cerebellum. *Trends Neurosci*. 2011;34:134-142.
7. Aruga J, Inoue T, Hoshino J, Mikoshiba K. Zic2 controls cerebellar development in cooperation with Zic1. *J Neurosci*. 2002;22:218-225.

8. Selvadurai HJ, Mason JO. Wnt/beta-catenin signalling is active in a highly dynamic pattern during development of the mouse cerebellum. *PLoS One*. 2011;6:e23012.
9. Yang H, Zhu Q, Cheng J, et al. Opposite regulation of Wnt/beta-catenin and Shh signaling pathways by Rack1 controls mammalian cerebellar development. *Proc Natl Acad Sci U S A*. 2019;116:4661-4670.
10. Huang J, Shi T, Ma T, et al. CCDC134, a novel secretory protein, inhibits activation of ERK and JNK, but not p38 MAPK. *Cell Mol Life Sci*. 2008;65:338-349.
11. Huang J, Xiao L, Gong X, et al. Cytokine-like molecule CCDC134 contributes to CD8+ T-cell effector functions in cancer immunotherapy. *Cancer Res*. 2014;74:5734-5745.
12. Zhong J, Zhao M, Luo Q, et al. CCDC134 is down-regulated in gastric cancer and its silencing promotes cell migration and invasion of GES-1 and AGS cells via the MAPK pathway. *Mol Cell Biochem*. 2013;372:1-8.
13. Huang J, Zhang L, Liu W, et al. CCDC134 interacts with hADA2a and functions as a regulator of hADA2a in acetyltransferase activity, DNA damage-induced apoptosis and cell cycle arrest. *Histochem Cell Biol*. 2012;138:41-55.
14. Yu B, Zhang T, Xia P, Gong X, Qiu X, Huang J. CCDC134 serves a crucial role in embryonic development. *Int J Mol Med*. 2018;41:381-390.
15. Tronche F, Kellendonk C, Kretz O, et al. Disruption of the glucocorticoid receptor gene in the nervous system results in reduced anxiety. *Nat Genet*. 1999;23:99-103.
16. Muhammad T, Ali T, Ikram M, Khan A, Alam SI, Kim MO. Melatonin rescue oxidative stress-mediated neuroinflammation/ neurodegeneration and memory impairment in scopolamine-induced amnesia mice model. *J Neuroimmune Pharmacol*. 2019;14:278-294.
17. Yoon JH, Abdelmohsen K, Kim J, et al. Scaffold function of long non-coding RNA HOTAIR in protein ubiquitination. *Nat Commun*. 2013;4:2939.
18. Brown AS, Meera P, Altindag B, et al. MTSS1/Src family kinase dysregulation underlies multiple inherited ataxias. *Proc Natl Acad Sci U S A*. 2018;115:E12407-E12416.
19. Zhang K, Zhang Y, Gu L, et al. Islr regulates canonical Wnt signaling-mediated skeletal muscle regeneration by stabilizing Dishevelled-2 and preventing autophagy. *Nat Commun*. 2018;9:5129.
20. Elgendy M, Ciro M, Hosseini A, et al. Combination of hypoglycemia and metformin impairs tumor metabolic plasticity and growth by modulating the PP2A-GSK3β-MCL-1 Axis. *Cancer Cell*. 2019;35:798-815.
21. Bok S, Shin DY, Yallowitz AR, et al. MEKK2 mediates aberrant ERK activation in neurofibromatosis type I. *Nat Commun*. 2020;11:5704.
22. Choi BR, Cave C, Na CH, Sockanathan S. GDE2-dependent activation of canonical Wnt signaling in neurons regulates Oligodendrocyte maturation. *Cell Rep*. 2020;31:107540.
23. Gennarino VA, Singh RK, White JJ, et al. Pumilio1 haploinsufficiency leads to SCA1-like neurodegeneration by increasing wild-type Ataxin1 levels. *Cell*. 2015;160:1087-1098.
24. Karaca M, Maechler P. Development of mice with brain-specific deletion of floxed glud1 (glutamate dehydrogenase 1) using cre recombinase driven by the nestin promoter. *Neurochem Res*. 2014;39:456-459.
25. Mullen RJ, Buck CR, Smith AM. NeuN, a neuronal specific nuclear protein in vertebrates. *Development*. 1992;116:201-211.
26. Buffo A, Rossi F. Origin, lineage and function of cerebellar glia. *Prog Neurobiol*. 2013;109:42-63.
27. Hirano T. Regulation and interaction of multiple types of synaptic plasticity in a Purkinje neuron and their contribution to motor learning. *Cerebellum*. 2018;17:756-765.
28. Banerjee S, Alexander T, Majumdar D, et al. Loss of C/EBPdelta exacerbates radiation-induced cognitive decline in aged mice due to impaired oxidative stress response. *Int J Mol Sci*. 2019;20:885.
29. Sun Y, Jia L, Williams MT, et al. Temporal gene expression profiling reveals CEBPD as a candidate regulator of brain disease in prosaposin deficient mice. *BMC Neurosci*. 2008;9:76.
30. Zhang C, Ji Z, Wang M, et al. Stox1 as a novel transcriptional suppressor of Math1 during cerebellar granule neurogenesis and medulloblastoma formation. *Cell Death Differ*. 2016;23:2042-2053.
31. Lim J, Hao T, Shaw C, et al. A protein-protein interaction network for human inherited ataxias and disorders of Purkinje cell degeneration. *Cell*. 2006;125:801-814.
32. Servadio A, Koshy B, Armstrong D, Antalffy B, Orr HT, Zoghbi HY. Expression analysis of the ataxin-1 protein in tissues from normal and spinocerebellar ataxia type 1 individuals. *Nat Genet*. 1995;10:94-98.
33. Cunningham D, DeBarber AE, Bir N, et al. Analysis of hedgehog signaling in cerebellar granule cell precursors in a conditional Nsdhl allele demonstrates an essential role for cholesterol in postnatal CNS development. *Hum Mol Genet*. 2015;24:2808-2825.
34. Lordkipanidze T, Dunaevsky A. Purkinje cell dendrites grow in alignment with Bergmann glia. *Glia*. 2005;51:229-234.
35. Xu H, Yang Y, Tang X, et al. Bergmann glia function in granule cell migration during cerebellum development. *Mol Neurobiol*. 2013;47:833-844.
36. Sergaki MC, Guillemot F, Matsas R. Impaired cerebellar development and deficits in motor coordination in mice lacking the neuronal protein BM88/Cend1. *Mol Cell Neurosci*. 2010;44:15-29.
37. Bizzoca A, Virgintino D, Lorusso L, et al. Transgenic mice expressing F3/contactin from the TAG-1 promoter exhibit developmentally regulated changes in the differentiation of cerebellar neurons. *Development*. 2003;130:29-43.
38. Coluccia A, Tattoli M, Bizzoca A, et al. Transgenic mice expressing F3/contactin from the transient axonal glycoprotein promoter undergo developmentally regulated deficits of the cerebellar function. *Neuroscience*. 2004;123:155-166.
39. Sebastian AG, Claudia AV, Annette MV, et al. Behavioral phenotyping of nestin-Cre mice: implications for genetic mouse models of psychiatric disorders. *J Psychiatr Res*. 2014;55:87-95.
40. Chen SH, Lu CH, Tsai MJ. TCTP is essential for cell proliferation and survival during CNS development. *Cell*. 2020;9:133.
41. Wu Q, Hao Q, Li H, et al. Brain iron deficiency and affected contextual fear memory in mice with conditional Ferroportin1 ablation in the brain. *The FASEB J*. 2021;35:e21174.
42. Ciani L, Salinas PC. WNTs in the vertebrate nervous system: from patterning to neuronal connectivity. *Nat Rev Neurosci*. 2005;6:351-362.
43. Parr BA, Shea MJ, Vassileva G, McMahon AP. Mouse Wnt genes exhibit discrete domains of expression in the early embryonic CNS and limb buds. *Development*. 1993;119:247-261.
44. Pei Y, Brun SN, Markant SL, et al. WNT signaling increases proliferation and impairs differentiation of stem cells in the developing cerebellum. *Development*. 2012;139:1724-1733.
45. Oliver G, Mailhos A, Wehr R, Copeland NG, Jenkins NA, Gruss P. Six3, a murine homologue of the sine oculis gene, demarcates the most anterior border of the developing neural plate and is expressed during eye development. *Development*. 1995;121:4045-4055.
46. Lagutin OV, Zhu CC, Kobayashi D, et al. Six3 repression of Wnt signaling in the anterior neuroectoderm is essential for vertebrate forebrain development. *Genes Dev*. 2003;17:368-379.
47. Geng X, Speirs C, Lagutin O, et al. Haploinsufficiency of Six3 fails to activate sonic hedgehog expression in the ventral forebrain and causes holoprosencephaly. *Dev Cell*. 2008;15:236-247.
48. Shimomura Y, Agalliu D, Vonica A, et al. APCDD1 is a novel Wnt inhibitor mutated in hereditary hypotrichosis simplex. *Nature*. 2010;464:1043-1047.
49. Liao XH, Nguyen H. Epidermal expression of Lgr6 is dependent on nerve endings and Schwann cells. *Exp Dermatol*. 2014;23:195-198.

50. Banfi S, Servadio A, Chung MY, et al. Identification and characterization of the gene causing type 1 spinocerebellar ataxia. *Nat Genet*. 1994;7:513-520.

SUPPORTING INFORMATION

Additional supporting information may be found in the online version of the article at the publisher's website.

How to cite this article: Yin S, Liao Q, Wang Y, et al. *Ccdc134* deficiency impairs cerebellar development and motor coordination. *Genes, Brain and Behavior*. 2021;20(7):e12763. https://doi.org/10.1111/gbb.12763